Fast vortex wall motion in wide permalloy strips from double switching of the vortex core

Virginia Estévez and Lasse Laurson

COMP Centre of Excellence and Helsinki Institute of Physics, Department of Applied Physics, Aalto University,
P.O. Box 11100, FI-00076 Aalto, Espoo, Finland

We study vortex domain wall dynamics in wide permalloy strips driven by applied magnetic fields and spin-polarized electric currents. As recently reported [V. Estévez and L. Laurson, Phys. Rev. B **93**, 064403 (2016)], for sufficiently wide strips and above a threshold field, periodic dynamics of the vortex core are localized in the vicinity of one of the strip edges, and the velocity drop typically observed for narrow strips is replaced by a high-velocity plateau. Here, we analyze this behavior in more detail by means of micromagnetic simulations. We show that the high-velocity plateau originates from a repeated double switching of the magnetic vortex core, underlying the periodic vortex core dynamics in the vicinity of the strip edge, i.e., the "attraction-repulsion" effect. We also discuss the corresponding dynamics driven by spin-polarized currents, as well as the effect of including quenched random structural disorder to the system.

I. INTRODUCTION

In the past decade, domain wall (DW) dynamics in ferromagnetic nanostructures have received considerable attention, especially due to technological applications in spintronics, including memory [1,2] and logic devices [3–5]. Typically, DW dynamics in nanostrips and wires is induced by external magnetic fields [6–16] or spin-polarized electric currents [17–22]. Details of the resulting DW dynamics depend on the DW structure, which in turn depends on the material and geometry being considered. For materials with a high perpendicular magnetic anisotropy [23,24], the typical DW structures are of the Bloch and/or Néel type. On the other hand, for soft magnetic materials such as permalloy, the negligible magnetocrystalline anisotropy implies that the physics of the system is dictated by the competition between exchange interactions and shape anisotropy due to magnetostatic effects. The resulting in-plane domains along the long axis of the strip are separated by DWs with equilibrium structures ranging from relatively simple transverse and vortex DWs to more complex multi-vortex walls when increasing the strip width from tens and hundreds of nanometers towards several micrometers [8,9,25–27].

Most of the previous works related to in-plane materials have focused on the study of DW dynamics in narrow permalloy strips where the equilibrium DW structure is the transverse or vortex wall [7–12,28–31]. The DW dynamics for these systems is characterized by the emergence of an instability, often referred to as the Walker breakdown [32], which appears when the DW internal degrees of freedom are excited by a strong enough external driving force. The Walker breakdown occurs for both magnetic fields B_{ext} above the Walker field B_W and spin-polarized current densities J exceeding the Walker current density J_W [7,10,14,33]. For low magnitudes of the driving force, i.e., within the steady or viscous regime, the DW propagation velocity increases monotonically up to $B_{ext} = B_W$ or $J = J_W$. Above the Walker breakdown, DW velocity drops abruptly as a consequence of the periodic transitions between different DW structures. For narrow strips with transverse DWs, repeated transitions between the transverse DW and a dynamic structure with

an antivortex propagating across the strip width occur [9]. For slightly wider strips (typically in the range of 200 to 300 nm) with vortex wall as the equilibrium DW structure, similar periodic transitions between different DW structures including vortex, transverse, and antivortex DWs have been observed [9,28].

Recently, we have shown that DW dynamics in even wider permalloy strips, with strip widths ranging from a few hundred nanometers to a few micrometers, display a multitude of regimes, depending on the geometry of the system, as well as on the magnitude of the applied magnetic field [16]. These include, e.g., transitions between various DW structures, and the fact that for some combinations of the strip geometry and the applied field the system cannot support a compact DW. The dynamics of multivortex DWs (double and triple vortex DWs [16]) is controlled by the polarities of the vortices. One of the most interesting behaviors characteristic of wide enough strips is an oscillatory motion of the vortex core close to one of the strip edges, which we refer to as the *attraction-repulsion effect* [16]. There, the vortex core first approaches the strip edge driven by the gyrotropic force, followed by a reversal of propagation direction as the core is pushed back towards the middle of the strip. Then, the core starts another approach towards the same strip edge, and the process repeats itself. Due to this effect the velocity drop typically associated with a Walker breakdown is absent in wide strips, leading instead to an extended high-velocity plateau in the velocity-field curve [16]. Somewhat similar absence of the velocity drop has been previously observed in systems with a high perpendicular anisotropy and a finite Dzyaloshinskii-Moriya interaction [34], as well as in ferromagnetic nanotubes [35]. However, many details of the attraction-repulsion effect are not fully understood, and thus more studies are required.

In this paper, we provide a complete description of the attraction-repulsion effect of vortex DW dynamics by micromagnetic simulations. We analyze in detail the behavior when the DW dynamics is induced by an external magnetic field, and also consider the corresponding DW dynamics driven by spin-polarized electric currents. We also address the question of how the presence of quenched structural random disorder,
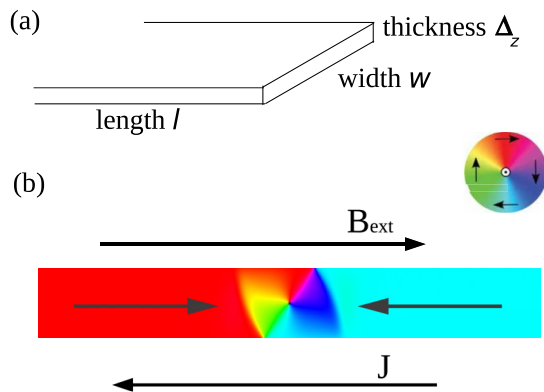
FIG. 1. (a) Geometry of the permalloy strip. (b) A top view of the magnetization in the initial state. Magnetization points along the long axis of the strip within the two domains (as indicated by the arrows) forming a head-to-head configuration. These domains are separated by a vortex DW. To study the DW dynamics, an external drive, i.e., either a magnetic field B_{ext} or a spin-polarized electric current density J is applied along the long axis of the strip.

originating, e.g., from the polycrystalline structure of the strips, affects the behavior. We find that the attraction-repulsion effect arises due to repeated double switching of the magnetic vortex core in the vicinity of one of the strip edges, both for field and current drive. Although structural disorder affects the DW dynamics in these systems, the attraction-repulsion effect is stable against structural disorder of moderate strength.

The paper is organized as follows: Section II describes the system under study and the main features of our micromagnetic simulations. Section III discusses in detail the attraction-repulsion effect when the DW dynamics is driven by an external magnetic field. DW dynamics driven by spin-polarized electric current in wide permalloy strips is described in Sec. IV, while Sec. V is dedicated to the effect of structural disorder on the DW dynamics. The conclusions and a summary of the main results are given in Sec. VI.

II. MICROMAGNETIC SIMULATIONS

The system analyzed is a permalloy strip of width w and thickness Δ_z, satisfying $\Delta_z \ll w$; see Fig. 1(a). DW dynamics is studied by micromagnetic simulations, where to mimic an infinitely long strip, the magnetic charges are compensated on the left and right ends of the strip. We consider the length l of the strip depending on the simulation window. For systems analyzed with a window moving with and centered at the DW, the length satisfies $l \geqslant 16w$. For a fixed simulation window we consider $l \geqslant 60w$. The initial state is an in-plane head-to-head equilibrium DW structure separating the two head-to-head domains; see Fig. 1(b). The equilibrium DW structure in general depends on w and Δ_z [9,26] and is the DW structure with the lowest energy for a given system. Here, the vortex wall is the equilibrium DW structure for all w and Δ_z values considered [26]. Starting from such an equilibrium state, DW dynamics is induced by applying either an external magnetic field B_{ext} or a spin-polarized current density J; see Fig. 1(b). All the results presented in this work have been calculated for the typical material parameters of permalloy,

i.e., saturation magnetization $M_s = 860 \times 10^3$ A/m, exchange constant $A_{ex} = 13 \times 10^{-12}$ J/m, and the Gilbert damping constant $\alpha = 0.01$. We analyze two different systems, the ideal case of strips free of any structural disorder or impurities and strips with structural disorder. In the simulations the disorder is introduced by Voronoi tessellation [15,36–38] to mimic effects due to the polycrystalline structure of the strip, as is explained in more detail in Sec. V. For all simulations we set the temperature T equal to zero.

The simulations are performed using the GPU-accelerated micromagnetic code MuMax3 [39–41], offering a significant speedup as compared to CPU codes for the large system sizes we consider here. The magnetization dynamics of the system is calculated numerically by the Landau-Lifshitz-Gilbert (LLG) equation [42,43],

$$\partial \mathbf{m}/\partial t = \gamma \mathbf{H}_{eff} \times \mathbf{m} + \alpha \mathbf{m} \times \partial \mathbf{m}/\partial t, \qquad (1)$$

where $\mathbf{m}$ is the magnetization, γ the gyromagnetic ratio, and $\mathbf{H}_{eff}$ the effective field, with contributions due to exchange, Zeeman, and demagnetizing energies. The discretization cell used depends on the system size, but is always bounded from above by the exchange length, $\Lambda = (2A/\mu_0 M_s^2)^{1/2} \approx 5$ nm, in the in-plane directions, and equals Δ_z in the out-of-plane direction.

III. MAGNETIC FIELD DRIVEN DW DYNAMICS

As the attraction-repulsion effect is a behavior observed in the vortex DW dynamics, we restrict the study to strips with geometries where the vortex DW is the equilibrium DW structure [26]. The vortex DW is characterized by the core polarity p, and chirality C, or the sense of in-plane rotation around the core. The polarity is given by the sign of the out-of-plane magnetization of the core, and can thus be up or down, corresponding to $p = \pm 1$. C is defined as clockwise ($C = -1$) or counterclockwise ($C = +1$) rotation of the in-plane magnetization around the core. A clockwise VW with $C = -1$ and $p = -1$ is represented in Fig. 1(b).

For reference, we first review the typical dynamical behavior for field-driven vortex DW dynamics in narrow permalloy strips. Figure 2(a) shows the DW velocity v as a function of the applied magnetic field B_{ext} for three different strip geometries. In the case of a narrow strip of width $w = 240$ nm and thickness $\Delta_z = 20$ nm, a steady and viscous low-field regime with v increasing roughly linearly with B_{ext} up to the Walker field B_W is observed. In this regime, the motion of the vortex DW occurs with the vortex core displaced from its equilibrium position in the middle of the strip, with the displacement increasing with B_{ext}. For $B_{ext} > B_W$, v drops abruptly as a consequence of the onset of periodic transformations between different DW structures. For example, for $B_{ext} = 1.5$ mT, the vortex core repeatedly moves across the strip width from one edge to the other, leading to periodic transformations between vortex and transverse DW structures. The corresponding trajectory (y coordinate) y_c of the vortex core is shown in Fig. 2(b). The vortex core first approaches one of the strip edges and exits the strip when reaching the edge. It is subsequently injected back into the system with a reversed polarity, after which it moves towards the other edge, and the process repeats itself.
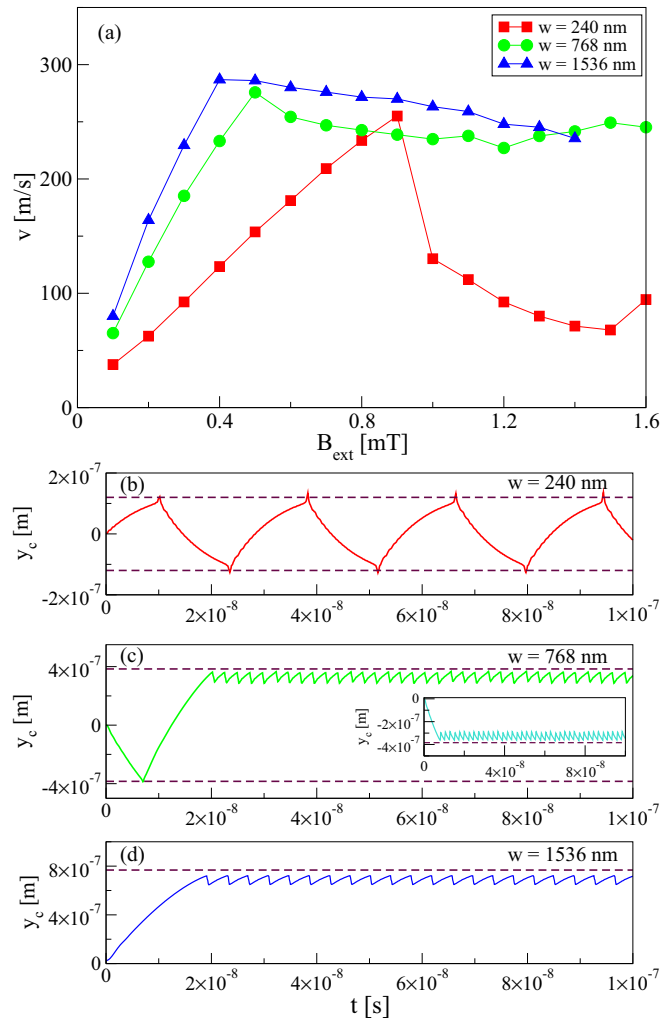
FIG. 2. (a) $v(B_{ext})$ curves for different strip geometries, where the vortex wall is the equilibrium DW structure. (b)–(d) The trajectory y_c of the vortex core for the systems shown in (a) at a given external field. The dashed lines represent the strip edges. (b) $w = 240$ nm, $\Delta_z = 20$ nm, and $B_{ext} = 1.5$ mT. The vortex core moves repeatedly across the strip from one edge to the other. In wider strips, the attraction-repulsion effect takes place: (c) $w = 768$ nm, $\Delta_z = 15$ nm, and $B_{ext} = 1.5$ mT. The main panel shows the trajectory of the core of a clockwise vortex, while the inset displays the corresponding $y_c(t)$ for the core of a counter-clockwise vortex. (d) $w = 1536$ nm, $\Delta_z = 15$ nm, and $B_{ext} = 0.7$ mT. $y_c = 0$ corresponds to the initial equilibrium state with the vortex core in the middle of the strip; see Fig. 1(b).

For wider strips, the $v(B_{ext})$ curve is very different to the one found for narrow systems; see Fig. 2(a), which also shows the $v(B_{ext})$ curves for two different wider strips. These curves have been reproduced here for reference from our recent paper [16]. The two wide strips considered have the same thickness $\Delta_z = 15$ nm and different widths, $w = 768$ nm and $w = 1536$ nm. As in the case of narrow strips, for low fields v displays a linear dependence on B_{ext} within the steady or viscous regime. However, above this regime, a high-velocity plateau is observed in the $v(B_{ext})$ curve, instead of the velocity drop found for narrow strips. A similar plateau was previously obtained experimentally and numerically [13,29]. The existence of this plateau was associated with the fact that in this regime the vortex cannot leave the system through one of the edges of the strip [13]. However, we have recently shown that the reason for these large v values is the attraction-repulsion effect [16]. This behavior avoids the periodic transformations between different DW structures that reduce the DW propagation velocity above the Walker field H_W in narrow strips. Moreover, for wide strips the vortex core is not able to leave the strip. For some reason, the vortex core is pushed back a small distance inside the strip before reaching the strip edge and subsequently starts a new approach towards the same edge, before being pushed back again (see also movie 1 provided as Supplemental Material [44]). Thus, the vortex core exhibits periodic oscillations confined within the vicinity of one of the edges of the strip. As a result, the dynamics involving transformations between different DW structures found in narrow strips do not occur, and the velocity drop is absent; see Figs. 2(c) and 2(d).

A closer look reveals further details of this process. From the trajectory y_c represented in the main panel of Fig. 2(c), it is evident that the vortex core first moves to the bottom edge, leaves the strip without any problem (i.e., no attraction-repulsion effect takes place), is injected back into the system (with a reversed polarity), moves towards the top edge, and experiences the attraction-repulsion effect there. Thus, the attraction-repulsion effect only occurs in one of the edges of the strip. We find that the edge where this effect occurs depends on the vortex chirality C and the direction of the applied magnetic field (positive or negative x direction). For the same strip geometry and applied field, the vortex oscillations of the attraction-repulsion effect take place close to the top or bottom edge depending on the chirality of the vortex. In Fig. 2(c), the main panel corresponds to a clockwise vortex ($C = -1$), whereas the inset shows the trajectory of a counterclockwise ($C = +1$) vortex.

To understand this, we start by considering the counterclockwise vortex represented schematically in Fig. 3(a). Similar ideas to explain the fact that the vortex core cannot leave the system through one of the strip edge have been presented by Zinoni *et al.* [13]. In Fig. 3, a full circle represents the vortex core, and the empty ones denote the half-antivortex edge defects. When the field is applied, the vortex core moves in the trajectory between the two edge defects, represented by the dashed line. If the vortex goes to the bottom edge, the area of the vortex structure with magnetization parallel to the applied field decreases, leading to a cost in Zeeman energy that prevents the exit of the core [13]. Instead, when the vortex moves towards the top edge the region with the vortex magnetization antiparallel to the field shrinks, while the parallel area increases, facilitating the core expulsion off the strip. Analogously, for a clockwise vortex [see Fig. 3(b)], the area of the vortex magnetization parallel to B_{ext} decreases when the vortex moves towards the top edge. Thus, the edge in the neighborhood of which the attraction-repulsion effect occurs is different depending on the vortex chirality. If the magnetic field is applied in the opposite sense, the strip edge associated with the attraction-repulsion effect changes for a given chirality. One should note that the relation between the chirality and the field is the same in narrow and wide strips. However, the significant energy cost preventing the expulsion of the vortex is only characteristic of wide enough
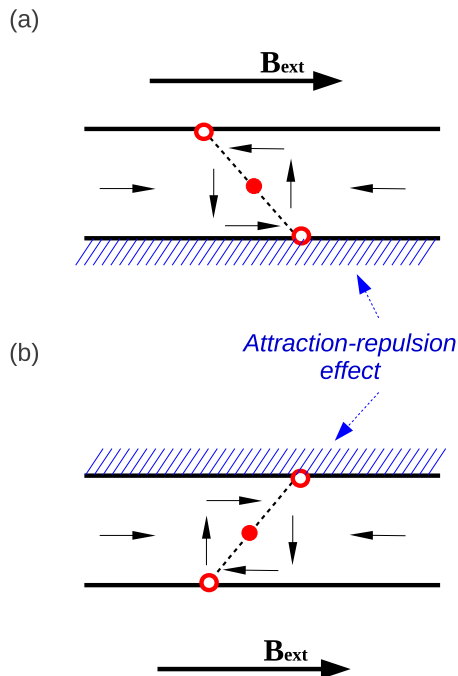
(a)

(b)

FIG. 3. Top view sketch of the vortex DW structures, indicating the strip edge where the attraction-repulsion effect takes place depending on the chirality of the vortex. (a) Counterclockwise chirality. (b) Clockwise chirality. Vortex core and the half-antivortex edge defects are denoted by filled and open circles, respectively.
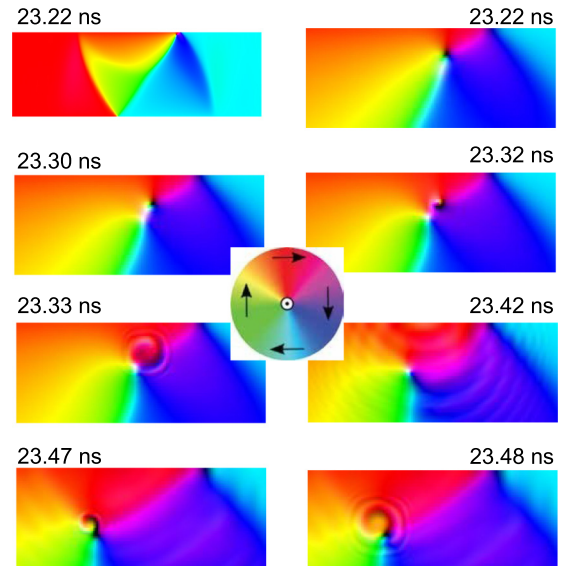

FIG. 4. A sequence of magnetization snapshots with a high temporal resolution showing the different stages of the fast double switching event underlying the attraction-repulsion effect. Here, $B_{ext} = 0.7$ mT in a strip with $w = 1536$ nm and $\Delta_z = 15$ nm is considered. The top-left panel shows the whole vortex wall, while the other panels are magnifications of the region around the vortex core close to the top edge of the strip. The process consists of a formation of a dip particle, leading to the nucleation of a vortex-antivortex pair, followed by annihilation of the initial vortex and the antivortex (first switching). The second core switching is assisted by the spin waves generated in the annihilation process.

strips. This is due to shape anisotropy (understood here as the tendency of the magnetization to align along the long axis of the strip) being essentially an edge effect. While in narrow strips the shape anisotropy (or the magnetostatic energy) is more uniform throughout the whole strip, in wide strips shape anisotropy favoring magnetization to point along the strip axis is less important in the middle of the strip than close to the edges. As a result, in wide strips the energy required to push the vortex core out of the strip is larger than the energy needed to move the vortex core off its equilibrium position in the middle of the strip.

This argument explains why the vortex core cannot leave the strip. However, as we can see in Figs. 2(c) and 2(d), the oscillations occur in the vicinity of the strip edge, and in no case the vortex core arrives to the opposite edge. Thus, something is happening during the motion of the vortex core towards the opposite edge, leading to a reversal in the direction of motion. Moreover, for the case of a strip with $w = 768$ nm and $\Delta_z = 15$ nm, for some values of the field the attraction-repulsion effect occurs even if the vortex core leaves the strip for a short time. Thus, a pertinent question is: why does the core reverse its propagation direction back towards the strip edge?

When an external field is applied, the motion of the vortex core is controlled by the gyrotropic force [45] $\mathbf{F}^g = pG\hat{\mathbf{z}} \times \mathbf{v}$; here p is the polarity, G is the gyrotropic constant and $\mathbf{v}$ the velocity of the vortex core. For a given field along the long axis of the strip, depending on the polarity the vortex core moves towards the top or bottom edge of the strip. Thus, a change of direction in the motion of the vortex can only be

due to a change in the vortex polarity. Analyzing the DW dynamics with more precision (high temporal resolution), we have observed that the attraction-repulsion effect involves a double switching of the magnetic vortex core. Figure 4 shows the fast VW dynamics sequence during such a process for a strip with $w = 1536$ nm and $\Delta_z = 15$ nm for $B_{ext} = 0.7$ mT; see also movie 2 provided as Supplemental Material [44]. The top-left snapshot in Fig. 4 shows a top view of the strip where the vortex core is very close to the top edge of the strip, driven towards it by the gyrotropic force. Magnifying the area close to the vortex and the strip edge (top-right panel of Fig. 4) shows that close to the out-of-plane vortex core (black) appears an area with opposite out-of-plane magnetization (white). This deformation of the core is known as a dip particle [46,47]. With time this area increases and leads to the nucleation of a vortex-antivortex pair, with both the new vortex and antivortex having the same polarities, which is opposite to the polarity of the initial vortex (23.30 ns, Fig. 4). Next, a very fast annihilation process between the antivortex and the initial vortex occurs (23.32 ns, Fig. 4). Thus, the vortex remaining in the strip has the opposite polarity to the initial vortex, leading to a polarity switching of the vortex core. Consequently, the gyrotropic force changes direction, and the vortex core starts to move away from the strip edge. The vortex-antivortex annihilation process is followed by emission of spin waves [46,48–50] (23.33 ns, Fig. 4). This is due to violation of the conservation of the skyrmion charge, $q = np/2$, where n is the winding number [51], in the antiparallel annihilation process of the

vortex-antivortex pair. As a consequence of these spin waves, very close to the core of the remaining vortex, an area with out-of-plane magnetization opposite to that of the vortex core is created (23.42 ns, Fig. 4). This area grows, becoming larger than the vortex core. Soon after, the area wraps the vortex core by forming a spiral around it (23.47 ns, Fig. 4). This process not only produces more spin waves but also leads to the second switching of the vortex core polarity (23.48 ns, Fig. 4). This second reversal of the polarity occurs without the formation of a vortex-antivortex pair. Given the polarity of the vortex, the gyrotropic force now pushes the core towards the strip edge, and the process repeats itself.

We note that for some strip geometries and applied fields, for example, $w = 768$ nm, $\Delta_z = 15$ nm, and $B = 1$ mT, a similar process is found where no dip particle is formed. In this case, the first core switching takes place when the vortex core is able to exit the strip and is subsequently injected back with a reversed polarity. At the same time, there is injection of spin waves into the strip. This is then followed by the second reversal as described above for the "pure" attraction-repulsion effect, again leading to oscillatory vortex core dynamics localized to the neighborhood of one of the edges of the strip.

Thus, the attraction-repulsion effect involves a double switching of the magnetic vortex core. The first switching proceeds via the creation of a vortex-antivortex pair followed by an annihilation process. The second one appears to be due to the spin waves generated in this annihilation process. The reversal processes occur very fast, with the double switching time being ∼260 ps for the relatively low field considered here. This time depends slightly on the geometry of the strip and the magnitude of the driving field. Due to its importance in magnetic data storage, switching of the magnetic vortex core has been studied extensively, and may be excited by magnetic fields [46,47,52–56], spin-polarized electric currents [57–62], and spin waves [63–69]. The switching mechanism mediated by the vortex-antivortex pair is rather well-known. The creation of a dip particle leading to the nucleation of a vortex-antivortex pair has been associated with an effective field, the gyrofield, which depends on the vortex core velocity [47]. There is a widespread belief that the switching process occurs when the velocity of the vortex core reaches a critical "core-switching" velocity [62]. However, this is not true for all the cases. Several works [60,63,70] have shown that high velocity of the vortex core is not a necessary condition for core switching. Indeed, it has been shown that the vortex core reversal occurs when a well-defined threshold in the exchange energy density is reached, corresponding to the energy necessary for the production of a vortex-antivortex pair [71]. In our system, we have not observed a clear correlation between the velocity of the vortex core and its reversal, such that the velocity would increase prior to the switching event. In our case, the creation of the dip particle appears to be related to the fact that the vortex core cannot exit the strip due to increasing energy as the core approaches the strip edge. The core reversal would then serve as a mechanism to reduce the energy of the system.

To quantify this, Fig. 5 shows the time evolution of demagnetizing energy E_{demag}, the exchange energy E_{exch} and the total energy E_{tot} (with $E_{tot} = E_{demag} + E_{exch} + E_{Zeeman}$)
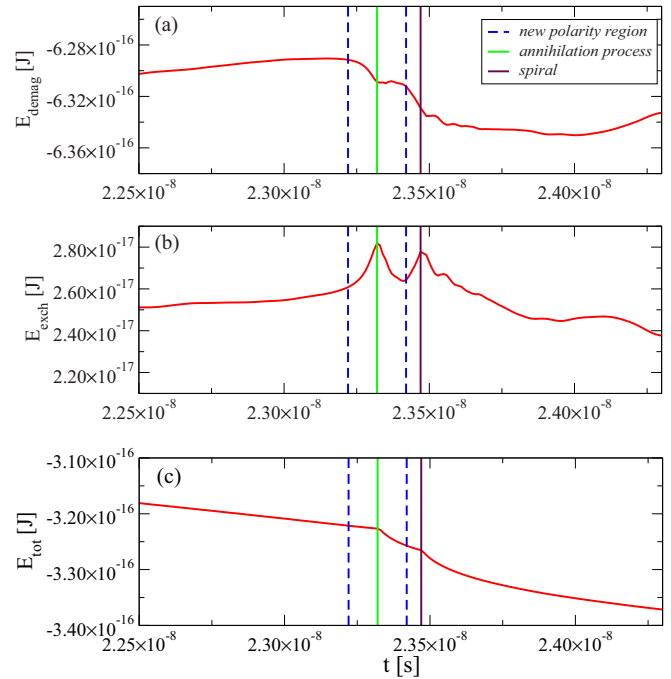

FIG. 5. Different energies of the system as a function of time during the double switching process portrayed in Fig. 4, with $w = 1536$ nm, $\Delta_z = 15$ nm, and $B_{ext} = 0.7$ mT. (a) E_{demag}. (b) E_{exch}. (c) $E_{tot} = E_{demag} + E_{exch} + E_{Zeeman}$.

during a double switching process for a strip with $w = 1536$ nm, $\Delta_z = 15$ nm, and $B_{ext} = 0.7$ mT. Comparing the times with those in Fig. 4, we can see that as the vortex core is approaching the strip edge, both E_{demag} and E_{exch} increase. In addition, as discussed above, also E_{Zeeman} increases locally as the vortex core is approaching the edge of the strip where the attraction-repulsion effect takes place (see again Fig. 3). The decreasing *global* E_{Zeeman} dominating the time-evolution of E_{tot} in Fig. 5 is a result of growth of the domain parallel to B_{ext} due to domain wall motion. It is known that the nucleation of vortex cores may decrease E_{demag} [56]. As can be observed in Fig. 5(a), when the dip particle is created, E_{demag} decreases until the annihilation process takes place. After that, the time-dependence of the demagnetizing energy displays a plateau, and decreases again when the new out-of-plane area is created close to the vortex core by the emission of spin waves. Simultaneously, E_{exch} increases when the areas with opposite polarity are created, and only decreases when the annihilation process and the second switching (spiral) occur; see Fig. 5(b). After the creation of the dip particle, E_{exch} increases as a consequence of the increased magnetization gradients due to the different (anti)vortex cores present in the strip after the nucleation. Although E_{exch} increases with the creation of areas with opposite polarity, after the double switching E_{exch} decreases. Figure 5(c) shows that the total energy E_{tot} decreases faster during the switching processes. Notice also that E_{demag} starts to increase again after the double switching process as the vortex core starts another approach towards the strip edge. Thus, in our system the formation of the dip particle, and the subsequent core reversal, is a mechanism of the system to decrease its energy.

IV. SPIN-POLARIZED CURRENT DRIVEN DW DYNAMICS

DW dynamics in conductive ferromagnetic strips can be driven also by spin-polarized electric currents [17–22]. So far, previous works have focused on narrow strips, and practically nothing is known about DW dynamics driven by spin-polarized electric currents in wide permalloy strips.

In general, the nature of the spin-polarized current is quite different from a magnetic field, thus leading to differences in the resulting DW dynamics. To study the DW dynamics driven by spin-polarized electric currents, the LLG equation is modified to read [21]

$$\partial \mathbf{m}/\partial t = \gamma \mathbf{H}_{\mathrm{eff}} \times \mathbf{m} + \alpha \mathbf{m} \times \partial \mathbf{m}/\partial t$$
$$- (\mathbf{u} \cdot \nabla)\mathbf{m} + \beta \mathbf{m} \times [(\mathbf{u} \cdot \nabla)\mathbf{m}], \quad (2)$$

where $\mathbf{u}$ is a vector in the direction of the electron flow given by $\mathbf{u} = JPg\mu_B/(2eM_s)$. e is the electric charge of the electron, P is the polarization, and β a nondimensional parameter describing the degree of nonadiabaticity of the spin-transfer torque. The nature of the DW dynamics depends strongly on β. Here, we analyze the DW dynamics for three cases, i.e., for $\beta = 0$, $\beta = \alpha$, and $\beta = 2\alpha$. For the polarization, we consider a typical value for the permalloy, $P = 0.56$. The direction of the current-induced DW motion is opposite to the current direction, and thus the spin-polarized current is applied along the long axis of the strip in the direction shown in Fig. 1(b).

First, we again review the well-known DW dynamics in narrow strips for reference. Inset of Fig. 6(a) shows the DW velocity v as a function of the current density J for a strip with $w = 240$ nm and $\Delta_z = 20$ nm, with the vortex DW the equilibrium DW structure. For low current densities, i.e., below the intrinsic pinning threshold [18,72], the velocity is equal to zero in the adiabatic case ($\beta = 0$). Above this depinning threshold, v increases with J, and for large enough J, exhibits a linear dependence on J. In this regime, the DW dynamics shows transformations between different DW structures, characteristic of the Walker breakdown. In the case of $\beta = 2\alpha$, for low J, v increases linearly up to the Walker current density J_{W} similarly to the field-driven case. For both nonadiabatic cases ($\beta = \alpha$ and $\beta = 2\alpha$), the velocity in this regime is given by $v = \beta u/\alpha$ [21]. Above J_{W}, the velocity drops but less dramatically than in the field-driven system; see the inset of Fig. 6(a) and Fig. 2(a). Above the Walker breakdown v increases roughly linearly with a different slope, with transformations between vortex and transverse DW structures taking place. The current density of the depinning threshold for $\beta = 0$ and the Walker current density J_{W} for $\beta = 2\alpha$ coincide. For $\beta = \alpha$, a linear relation $v \approx \beta u/\alpha$ is obtained for any J, and the vortex DW moves with the vortex core in the middle of the strip.

Next, we proceed to consider wider permalloy strips. For $\beta = \alpha$, the DW dynamics is the same as that found for narrow strips. In fact, the behavior for $\beta = \alpha$ is fully independent of the width of the strip, as can be seen in Fig. 6(b), where the $v(J)$ curves are shown for different strip geometries. Notice that we consider here the same strips as in the field-driven case: $w = 120$ nm and $\Delta_z = 20$ nm, as well as $w = 768$ nm and $w = 1536$ nm both with $\Delta_z = 15$ nm. Figure 6(c) shows the $v(J)$ curves for $\beta = 2\alpha$. For low values of J, the velocity shows a linear behavior independent of the strip width w. A key
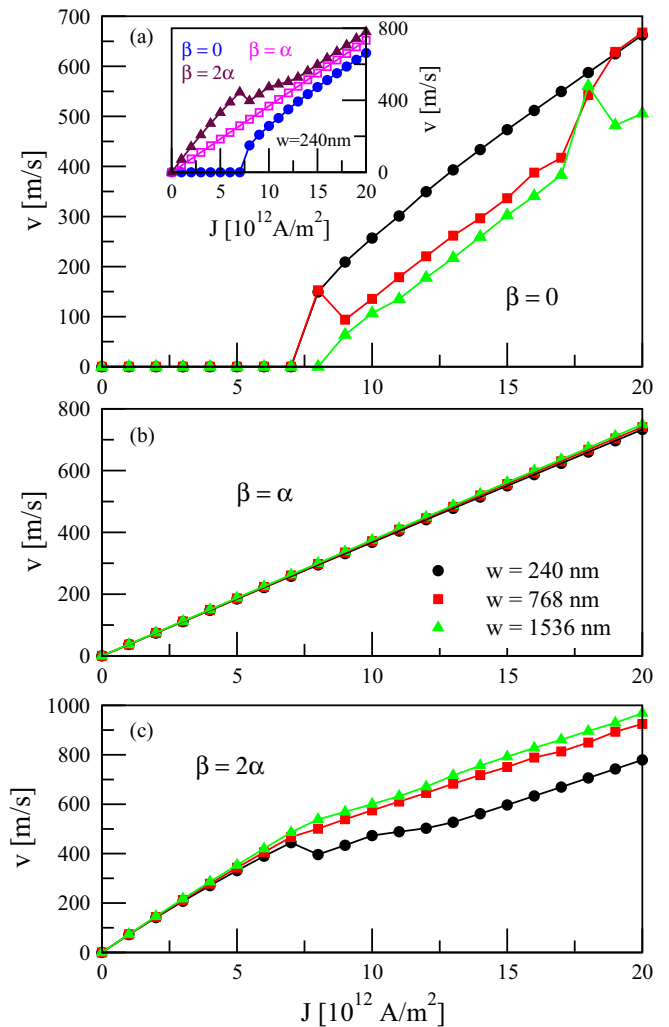

FIG. 6. Main figures: $v(J)$ curves for several values of β and different strip geometries, where vortex wall is the equilibrium DW structure. The widths of the strips considered are $w = 240$ nm, $w = 768$ nm, and $w = 1536$ nm. For $w = 240$ nm the thickness is $\Delta_z = 20$ nm, whereas for the other two strips $\Delta_z = 15$ nm. (a) $\beta = 0$. Inset: $v(J_{\mathrm{ext}})$ for a strip with $w = 240$ nm, $\Delta_z = 20$ nm, and several values of β. (b) $\beta = \alpha$. (c) $\beta = 2\alpha$.

point here is that in wider strips the velocity does not exhibit a drop as in the narrow case. Instead, there is a change in the slope of the $v(J)$ curve around the current density corresponding to J_{W} of the narrow system; see Fig. 6(c). As in the field-driven case, the underlying reason for this lack of velocity drop is the appearance of the attraction-repulsion effect. In the spin-polarized current driven case, the vortex core exits the strip more frequently than in the field-driven case. Only for some current densities for the widest strip ($w = 1536$ nm), the "pure" attraction-repulsion effect is observed. This is probably due to the spin-polarized current acting directly on the vortex core (or, more generally, large magnetization gradients), while the magnetic field acts more uniformly on the whole DW structure. As a result, the vortex core can leave the strip more easily in the spin-polarized current driven case. The trajectory y_c of the vortex core for a strip with $w = 768$ nm and $\Delta_z = 15$ nm is shown in Fig. 7(a) for $J = 12 \times 10^{12}$ A/m^2. The
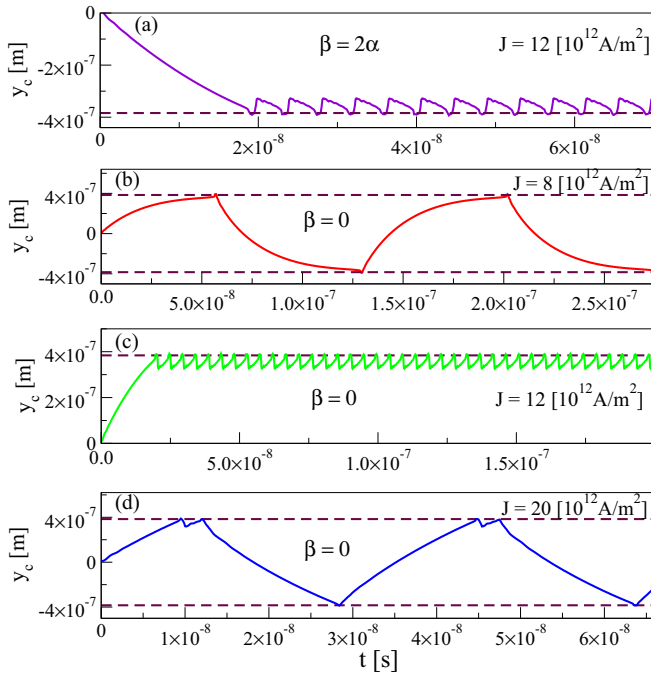
FIG. 7. Current-driven trajectories $y_c(t)$ of the vortex core for a strip with $w = 768$ nm and $\Delta_z = 15$ for different values of J and β. The dashed lines represent the strip edges. (a) $\beta = 2\alpha$ and $J = 12 \times 10^{12}$ A/m^2, showing the attraction-repulsion effect. (b)–(d) Trajectories for different regimes of behavior in the case of $\beta = 0$. (b) For $J = 8 \times 10^{12}$ A/m^2, the vortex core moves repeatedly across the strip from one edge to the other, showing the typical behavior above the Walker breakdown. (c) For $J = 12 \times 10^{12}$ A/m^2 the attraction-repulsion effect is observed. (d) For $J = 20 \times 10^{12}$ A/m^2, the trajectory displays a mixture between the transformations above the Walker breakdown and the attraction-repulsion effect. $y_c = 0$ corresponds to the initial equilibrium state with the vortex core in the middle of the strip.

attraction-repulsion effect occurs at the bottom edge as the DW structure studied in this case is a counterclockwise vortex DW. Depending on the value of J, the amplitude of the periodic oscillations can be smaller or larger. The larger the current density, the faster the double switching process.

For the adiabatic ($\beta = 0$) case considered in Fig. 6(a), different regimes of behavior occur above the depinning threshold when the width of the strip increases. The depinning threshold appears to increase slightly with the strip width. For strips with $w = 240$ nm and $w = 768$ nm, the depinning threshold is found to be the same, whereas for $w = 1536$ nm it is a little larger. For $J = 8 \times 10^{12}$ A/m^2 in the case of a strip with $w = 768$ nm, repeated transformations between vortex and transverse DW structures take place as in the case of narrow strips. The vortex core dynamics (the core trajectory y_c) in the former case is shown in Fig. 7(b). For 8×10^{12} A/m$^2 \leqslant J \leqslant 16 \times 10^{12}$ A/m^2, the vortex core moves to the strip edge and there is a kind of attraction-repulsion effect, with sometimes also a nucleation of an antivortex taking place. Contrary to the field-driven or the $\beta = 2\alpha$ case, when the DW dynamics presents this kind of attraction-repulsion effect v decreases with respect to the case in which there are transformations between DW structures.

The reduction of the velocity is due to the nucleation of an antivortex during the attraction-repulsion effect. Moreover, in this regime the velocity decreases with the strip width. For $\beta = 0$, when a spin-polarized current is applied, the vortex core moves in the opposite direction as compared to that of the field-driven or $\beta = 2\alpha$ case. Figures 7(a) and 7(c) show the $y_c(t)$ for the same strip for $J = 12 \times 10^{12}$ A/m^2 and $\beta = 2\alpha$ and $\beta = 0$, respectively. The same DW structure has been considered in both cases, i.e., a vortex DW with the same chirality and polarity. As can be seen, the vortex core motion in both cases is opposite even if the polarity is the same, and the attraction-repulsion effect occurs in different strip edges. Considering LLG equation with the spin transfer torque terms [72], the fourth term gives an opposite sign for the adiabatic case with respect to the nonadiabatic cases with $\beta > \alpha$. This is the reason why in the adiabatic ($\beta = 0$) case the vortex core moves to the opposite direction to that of the $\beta = 2\alpha$ case. For $J \geqslant 18 \times 10^{12}$ A/m^2 in the case of $w = 768$ nm, v experiences a large increase; see Fig. 6(a). In this regime the DW dynamics shows a combination of the transformations between DW structures and the attraction-repulsion effect; see Fig. 7(d), where the corresponding $y_c(t)$ curve is shown for $J = 20 \times 10^{12}$ A/m^2. The attraction-repulsion effect is observed also for $w = 1536$ nm. The combination of the attraction-repulsion effect and the transformations between DW structures only appears for $J = 18 \times 10^{12}$ A/m^2. This again illustrates the idea that as the strip width increases, the attraction-repulsion effect becomes increasingly prominent.

V. QUENCHED STRUCTURAL DISORDER

Although systems with disorder are more relevant experimentally, the effect of disorder on DW dynamics has in relative terms (as compared to the "pure" systems) received less attention in recent numerical studies [15,36,37,73,74]. Here, we analyze the effect of quenched structural disorder on the DW dynamics in wide permalloy strips, focusing on the attraction-repulsion effect. To simulate the polycrystalline structure of the material, the system is divided in different areas by Voronoi tessellation. Each area represents a grain. We consider a grain size equal to the thickness of the strip, and study the effect of the reduction of exchange coupling between grains, by means of a reduction of the exchange stiffness A_{exch} at the grain boundaries [37].

We start by considering the case in which the DW dynamics is driven by an external magnetic field. Contrary to the case of narrow strips where the vortex core often becomes pinned by disorder after some transient motion even for relatively large fields, for wide strips this is unusual. This is likely due to the fact that in wide strips the vortex core can follow several paths. Figure 8(a) shows the $v(B_{ext})$ curves for a strip with $w = 768$ nm, $\Delta_z = 15$ nm, and different reductions of the exchange coupling across the grain boundaries. As the vortex motion depends on the random disorder configuration, the velocity represented is the average over three different disorder realizations. For disorder of moderate strength (with a reduction of exchange stiffness equal to 20% or 30%), the velocity exhibits the characteristic plateau of the attraction-repulsion effect. The trajectories y_c of the vortex core show
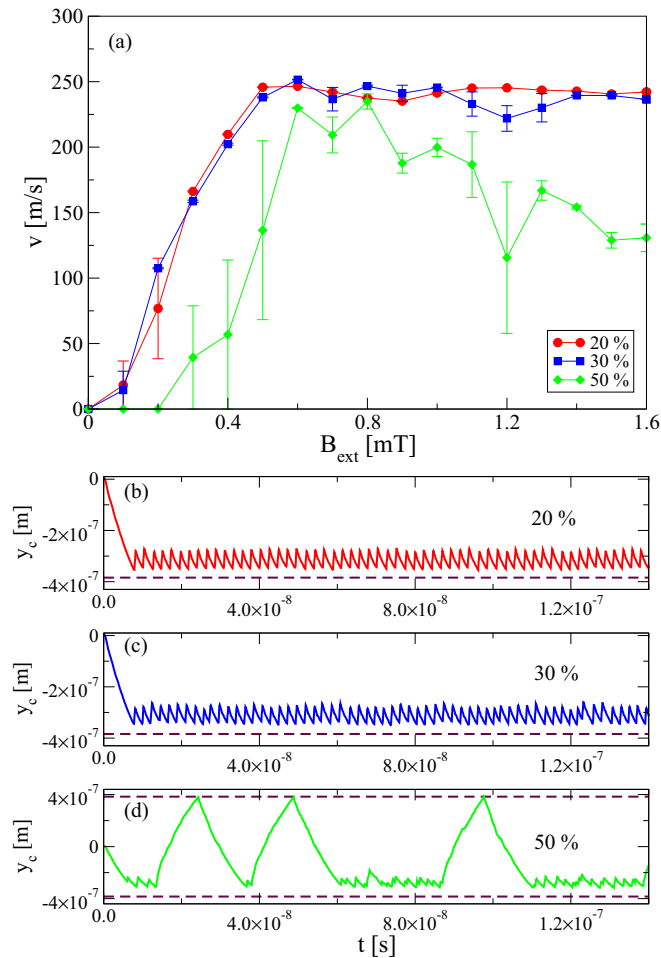
FIG. 8. (a) $v(B_{ext})$ curves for a strip with $w = 768$ nm and $\Delta_z = 15$ nm for different reductions of the exchange stiffness at the grain boundaries. (b)–(d) The trajectory y_c of the vortex core for the strip shown in (a) at $B_{ext} = 1.5$ mT for a reduction of the exchange stiffness of 20%, 30%, and 50%, respectively. The dashed lines represent the strip edges.

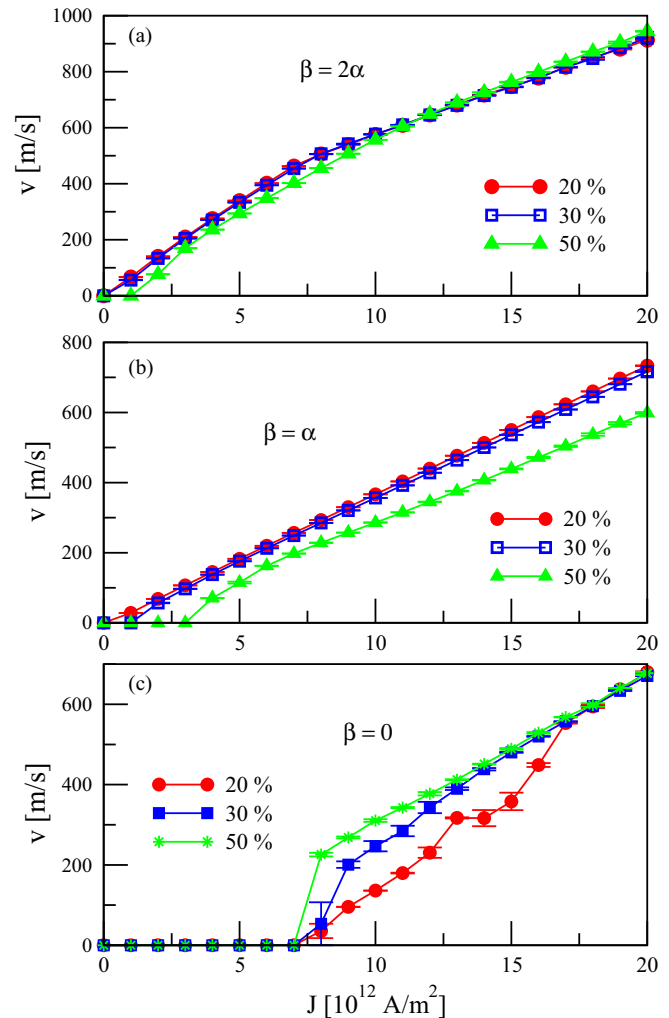

FIG. 9. $v(J)$ curves for a strip with $w = 768$ nm and $\Delta_z = 15$ nm, considering several values of β, and three different values for the reduction of A_{exch} at the grain boundaries. (a) $\beta = 2\alpha$. (b) $\beta = \alpha$. (c) $\beta = 0$.

oscillations close to the strip edge; see Figs. 8(b) and 8(c). As the disorder increases, the oscillations are more irregular. Thus, the attraction-repulsion effect is robust against disorder of moderate strength. However, for strong enough disorder, e.g., with an exchange reduction of 50%, the vortex motion reflects a combination of transformations between different DW structures and oscillations close to the border. This can be clearly seen in Fig. 8(d), where the trajectory of the vortex core is shown. As a consequence of this combination, the average DW velocity decreases. On the other hand, for strong disorder the DW becomes pinned for low fields; see Fig. 8(a).

For the case of DW dynamics driven by spin-polarized currents, the effect of disorder depends strongly on β. For $\beta = 2\alpha$, disorder barely affects the attraction-repulsion effect; see Fig. 9(a), where the $v(J)$ curves are represented for a strip with $w = 768$ nm, $\Delta_z = 15$ nm, and different reductions of the exchange coupling. As in the perfect case, there are two regimes of behavior, the steady state and the attraction-repulsion effect. The vortex core trajectory for this strip at $J = 15 \times 10^{12}$ A/m^2 and strong disorder is shown in Fig. 10(a).

Even for strong disorder the oscillations of the core position close to the strip edge are periodic. On the other hand, a finite "extrinsic" depinning threshold emerges for strong disorder (50%); see Fig. 9(a). The disorder affects slightly the slope of the velocity in the steady state. Moreover, the current density at which the regime with the attraction-repulsion effect starts is larger than in the case without disorder. For example, in a perfect strip with $J = 12 \times 10^{12}$ A/m^2 the attraction-repulsion effect is observed, whereas for a strip with strong disorder the dynamics is the typical one of the steady state. The disorder also softens the transition between the two regimes of behavior. At large values of J, v is almost independent of the disorder.

Also, for $\beta = \alpha$ and low values of J, a disorder-dependent depinning threshold is observed; see Fig. 9(b). The depinning threshold depends more strongly on the disorder strength than in the $\beta = 2\alpha$ case. Moreover, the velocity at a given J decreases with the disorder strength. For moderate disorder, the vortex dynamics is the same as that found in the perfect case. However, for strong disorder the vortex motion occurs
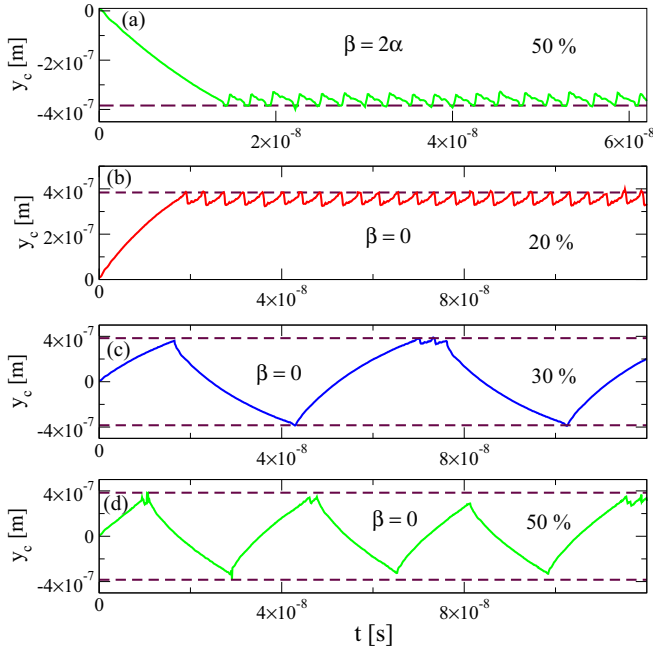
FIG. 10. Current-driven trajectories $y_c(t)$ of the vortex core for a strip with $w = 768$ nm and $\Delta_z = 15$ for different values of reduction of A_{exch} across the grain boundaries, and different β-values. The dashed lines represent the strip edges. (a) $\beta = 2\alpha$ and $J = 15 \times 10^{12}$ A/m^2 and an exchange stiffness reduction of 50%, showing the attraction-repulsion effect. (b)–(d) Trajectories for the same strip represented in (a) in the case of $\beta = 0$ and $J = 12 \times 10^{12}$ A/m^2 for different reductions of A_{exch}.

with the vortex core displaced from the equilibrium position in the middle of the strip. This can be related to an effective damping parameter α^* generated by the disorder, as occurs for the adiabatic case in strips with nonmagnetic voids [74].

For the adiabatic case ($\beta = 0$) the behavior is completely different from the rest of the cases. Curiously, the velocity at a given J increases with the disorder strength; see Fig. 9(c). For a reduction of 20%, there are two regimes of behavior. For 8×10^{12} A/m$^2 \leqslant J \leqslant 14 \times 10^{12}$ A/m^2 the vortex dynamics displays attraction-repulsion effect, while for $J \geqslant 15 \times 10^{12}$ A/m^2 a combination of the attraction-repulsion effect and transformations between different DW structures is observed. As J increases, transformations between the structures become the more prominent behavior. For 30% and 50%, transformations between different DW structures are the main behavior. This can be clearly seen in Figs. 10(b)–10(d), which show the vortex core trajectory for $J = 12 \times 10^{12}$ A/m^2 in a strip with $w = 768$ nm, $\Delta_z = 15$ nm, and exchange stiffness reductions of 20%, 30%, and 50%, respectively. For moderate disorder, the oscillations close to the strip edge are periodic and the attraction-repulsion effect is stable. For stronger disorder, the attraction-repulsion effect almost disappears, leading to transformations between DW structures. As we already saw for perfect strips, in the adiabatic case the velocity is larger when the dynamics shows the transformations between DW structures than when the attraction-repulsion effect takes place. As the disorder increases, the transformations between the DW structures are more favored than the attraction-repulsion

effect. For that reason, the velocity increases with the disorder. At high values of the spin-polarized current density, the velocity is independent of the magnitude of the structural disorder.

VI. SUMMARY AND CONCLUSIONS

To summarize, we have studied in detail the attraction-repulsion effect, an oscillatory motion of the vortex core localized close to one of the strip edges. This behavior, characteristic of wide permalloy strips, avoids the transformations between different DW structures, leading to a plateau-like regime with large values of the DW velocity, instead of the velocity drop observed in narrow strips. We have analyzed the attraction-repulsion effect when the DW dynamics is driven by an external magnetic field and also by spin-polarized electric currents. In both cases, we have seen that the origin of the oscillations is a repeated double switching of the magnetic vortex core. The first switching occurs via the creation of a vortex-antivortex pair, followed by an annihilation process. The second switching is assisted by the spin waves generated in the annihilation process. This double switching is a mechanism of the system to reduce its energy during the DW dynamics.

We have also studied the effect of quenched structural disorder on the DW dynamics in wide permalloy strips. Depending on the driving force (field or current) the disorder affects the DW dynamics in different ways. For the case of a magnetic field, the attraction-repulsion effect is robust against quenched structural disorder of moderate strength. For DW dynamics driven by spin-polarized electric currents, the degree of nonadiabaticity β plays an important role in the DW dynamics in disordered strips. For all values of β the vortex motion can be pinned at very low J due to the disorder. For $\beta = \alpha$, we have seen that the DW velocity at a fixed J decreases with the disorder strength. For $\beta = 2\alpha$, the attraction-repulsion effect is stable even in the case of strong disorder. However, in the adiabatic case ($\beta = 0$) the attraction-repulsion effect only occurs for weak disorder. Curiously and contrary to what happens in other cases where the attraction-repulsion effect leads to large values of the velocity, for $\beta = 0$ the DW velocity is larger when there are transformations between different DW structures. As a result, DW velocity at a given J increases with the disorder strength. Thus, for possible applications where stable and large values of the DW velocity as produced by the attraction-repulsion effect could be useful, the rather complex interplay of the details of the driving force and the disorder magnitude should be taken into account.

[1] S. S. P. Parkin, M. Hayashi, and L. Thomas, Science **320**, 190 (2008).

[2] S. E. Barnes, J. Ieda, and S. Maekawa, Appl. Phys. Lett. **89**, 122507 (2006).

[3] R. P. Cowburn and M. E. Welland, Science **287**, 1466 (2000).

[4] D. A. Allwood, G. Xiong, M. D. Cooke, C. C. Faulkner, D. Atkinson, N. Vernier, and R. P. Cowburn, Science **296**, 2003 (2002).

[5] D. A. Allwood, G. Xiong, C. C. Faulkner, D. Atkinson, D. Petit, and R. P. Cowburn, Science **309**, 1688 (2005).

[6] D. Atkinson, D. A. Allowood, G. Xiong, M. D. Cooke, C. C. Faulkner, and R. P. Cowburn, Nat. Mater. **2**, 85 (2003).

[7] G. S. D. Beach, C. Nistor, C. Knutson, M. Tsoi, and J. L. Erskine, Nat. Mater. **4**, 741 (2005).

[8] Y. Nakatani, A. Thiaville, and J. Miltat, J. Magn. Magn. Mater. **290-291**, 750 (2005).

[9] A. Thiaville and Y. Nakatani, in *Spin Dynamics in Confined magnetic Structures III*, edited by B. Hillebrands and A. Thiaville, Topics in Applied Physics, Vol. 101 (Springer, Berlin, 2006).

[10] M. Hayashi, L. Thomas, C. Rettner, R. Moriya, and S. S. P. Parkin, Nat. Phys. **3**, 21 (2007).

[11] J. Yang, C. Nistor, G. S. D. Beach, and J. L. Erskine, Phys. Rev. B **77**, 014413 (2008).

[12] R. Moriya, M. Hayashi, L. Thomas, C. Rettner, and S. S. P. Parkin, Appl. Phys. Lett. **97**, 142506 (2010).

[13] C. Zinoni, A. Vanhaverbeke, P. Eib, G. Salis, and R. Allenspach, Phys. Rev. Lett. **107**, 207204 (2011).

[14] M. Hayashi, L. Thomas, C. Rettner, R. Moriya, and S. S. P. Parkin, Appl. Phys. Lett. **92**, 112510 (2008).

[15] Y. Nakatani, A. Thiaville, and J. Miltat, Nat. Mater. **2**, 521 (2003).

[16] V. Estévez and L. Laurson, Phys. Rev. B **93**, 064403 (2016).

[17] M. Kläui, C. A. F. Vaz, J. A. C. Bland, W. Wernsdorfer, G. Faini, E. Cambril, and L. J. Heyderman, Appl. Phys. Lett. **83**, 105 (2003).

[18] A. Thiaville, Y. Nakayama, J. Miltat, and N. Vernier, J. Appl. Phys. **95**, 7049 (2004).

[19] M. Kläui, P.-O. Jubert, R. Allenspach, A. Bischof, J. A. C. Bland, G. Faini, U. Rüdiger, C. A. F. Vaz, L. Vila, and C. Vouille, Phys. Rev. Lett. **95**, 026601 (2005).

[20] N. Vernier, D. A. Allwood, D. Atkinson, M. D. Cooke, and R. P. Cowburn, Europhys. Lett. **65**, 526 (2004).

[21] A. Thiaville, Y. Nakatani, J. Miltat, and Y. Suzuki, Europhys. Lett. **69**, 990 (2005).

[22] A. Yamaguchi, T. Ono, S. Nasu, K. Miyake, K. Mibu, and T. Shinjo, Phys. Rev. Lett. **92**, 077205 (2004).

[23] K. H. J. Buschow and F. R. de Boer, *Physics of Magnetism and Magnetic Materials* (Kluwer Academic Press, New York, 2003).

[24] J. M. D. Coey, *Magnetism and Magnetic Materials* (Cambridge University Press, Cambridge, 2010).

[25] R. D. McMichael and M. J. Donahue, IEEE Trans. Magn. **33**, 4167 (1997).

[26] V. Estévez and L. Laurson, Phys. Rev. B **91**, 054407 (2015).

[27] M. Kläui, C. A. F. Vaz, J. A. C. Bland, L. J. Heyderman, F. Nolting, A. Pavlovska, E. Bauer, S. Cherifi, S. Heun, and A. Locatelli, Appl. Phys. Lett. **85**, 5637 (2004).

[28] J.-Y. Lee, K.-S. Lee, S. Choi, K. Y. Guslienko, and S. K. Kim, Phys. Rev. B **76**, 184408 (2007).

[29] K. Weerts, P. Neutens, L. Lagae, and G. Borghs, J. Appl. Phys. **103**, 094307 (2008).

[30] O. A. Tretiakov, D. Clarke, G.-W. Chern, Y. B. Bazaliy, and O. Tchernyshyov, Phys. Rev. Lett. **100**, 127204 (2008).

[31] D. J. Clarke, O. A. Tretiakov, G.-W. Chern, Y. B. Bazaliy, and O. Tchernyshyov, Phys. Rev. B **78**, 134412 (2008).

[32] N. L. Schryer and L. R. Walker, J. Appl. Phys. **45**, 5406 (1074).

[33] S. Glathe, R. Mattheis, and D. V. Berkov, Appl. Phys. Lett. **93**, 072508 (2008).

[34] A. Thiaville, S. Rohart, E. Jue, V. Cros, and A. Fert, Europhys. Lett. **100**, 57002 (2012).

[35] M. Yan, C. Andreas, A. Kakay, F. Garcia-Sanchez, and R. Hertel, Appl. Phys. Lett. **99**, 122505 (2011).

[36] J. Leliaert, B. Van de Wiele, A. Vansteenkiste, L. Laurson, G. Durin, L. Dupré, and B. Van Waeyenberge, Phys. Rev. B **89**, 064419 (2014).

[37] J. Leliaert, B. Van de Wiele, A. Vansteenkiste, L. Laurson, G. Durin, L. Dupré, and B. Van Waeyenberge, J. Appl. Phys. **115**, 233903 (2014).

[38] J. Leliaert, B. Van de Wiele, A. Vansteenkiste, L. Laurson, G. Durin, L. Dupré, and B. Van Waeyenberge, J. Appl. Phys. **115**, 17D102 (2014).

[39] http://mumax.github.io

[40] A. Vansteenkiste and B. Van de Wiele, J. Magn. Magn. Mater. **323**, 2585 (2011).

[41] A. Vansteenkiste *et al.*, AIP Adv. **4**, 107133 (2014).

[42] T. L. Gilbert, IEEE Trans. Magn. **40**, 3443 (2004).

[43] W. F. Brown, Jr., *Micromagnetics* (Wiley, New York, 1963).

[44] See Supplemental Material at http://link.aps.org/supplemental/10.1103/PhysRevB.96.064420 for movies illustrating the details of the domain wall dynamics discussed in the paper.

[45] A. P. Malozemoff and J. C. Slonczewski, *Magnetic Domain Wall in Bubble Materials* (Academic Press, New York, 1979).

[46] B. Van Waeyenberge, A. Puzic, H. Stoll, K. W. Chou, T. Tyliszczak, R. Hertel, M. Fähnle, H. Brückl, K. Rott, G. Reiss, I. Neudecker, D. Weiss, C. H. Back, and G. Schütz, Nature **444**, 461 (2006).

[47] K. Y. Guslienko, K.-S. Lee, and S.-K. Kim, Phys. Rev. Lett. **100**, 027203 (2008).

[48] K. S. Lee, S. Choi, and S. K. Kim, App. Phys. Lett. **87**, 192502 (2005).

[49] R. Hertel and C. M. Schneider, Phys. Rev. Lett. **97**, 177202 (2006).

[50] O. A. Tretiakov and O. Tchernyshyov, Phys. Rev. B **75**, 012408 (2007).

[51] O. Tchernyshyov and G.-W. Chern, Phys. Rev. Lett. **95**, 197204 (2005).

[52] A. Vansteenkiste, K. W. Chou, M. Weigand, M. Curcic, V. Sackmann, H. Stoll, T. Tyliszczak, G. Woltersdorf, C. H. Black, G. Shütz, and B. Van Waeyenberge, Nat. Phys. **5**, 332 (2009).

[53] R. Hertel, S. Gliga, M. Fähnle, and C. M. Schneider, Phys. Rev. Lett. **98**, 117201 (2007).

[54] K.-S. Lee, K. Y. Guslienko, J.-Y. Lee, and S. K. Kim, Phys. Rev. B **76**, 174410 (2007).

[55] S.-K. Kim, J.-Y. Lee, Y.-S. Choi, K. Y. Guslienko, and K. S. Lee, Appl. Phys. Lett. **93**, 052503 (2008).

[56] Q. F. Xiao, J. Rudge, B. C. Choi, Y. K. Hong, and G. Donohoe, Appl. Phys. Lett. **89**, 262507 (2006).

[57] Y. Liu, S. Gliga, R. Hertel, and C. M. Schneider, Appl. Phys. Lett. **91**, 112501 (2007).

[58] K. Yamada, S. Kasai, Y. Nakatani, K. Kobayashi, H. Kohno, A. Thiaville, and T. Ono, Nat. Mater. **6**, 270 (2007).

[59] K. Yamada, S. Kasai, Y. Nakatani, K. Kobayashi, and T. Ono, Appl. Phys. Lett. **93**, 152502 (2008).

[60] K. Yamada, S. Kasai, Y. Nakatani, K. Kobayashi, and T. Ono, Appl. Phys. Lett. **96**, 192508 (2010).

[61] J.-G. Caputo, Y. Gaididei, F. G. Mertens, and D. D. Sheka, Phys. Rev. Lett. **98**, 056604 (2007).

[62] S.-K. Kim, Y.-S. Choi, K.-S. Lee, K. Y. Guslienko, and D.-E. Jeong, Appl. Phys. Lett. **91**, 082506 (2007).

[63] M. Kammerer, M. Weigand, M. Curcic, M. Noske, M. Sproll, A. Vansteenkiste, B. Van Waeyenberge, H. Stoll, G. Woltersdorf, G. Woltersdorf, C. Back, and G. Schütz, Nat. Commun. **2**, 279 (2011).

[64] M. Kammerer, H. Stoll, M. Noske, M. Sproll, M. Weigand, C. Illg, G. Woltersdorf, M. Fähnle, C. Back, and G. Schütz, Phys. Rev. B **86**, 134426 (2012).

[65] M. Noske, H. Stoll, M. Fähnle, A. Gangwar, G. Woltersdorf, A. Slavin, M. Weigand, G. Dieterle, J. Föster, C. Back, and G. Schütz, J. Appl. Phys. **119**, 173901 (2016).

[66] J. P. Park and P. A. Crowell, Phys. Rev. Lett. **95**, 167201 (2005).

[67] H. G. Bauer, M. Sproll, C. H. Back, and G. Woltersdorf, Phys. Rev. Lett. **112**, 077201 (2014).

[68] M.-W. Yoo, J. Lee, and S.-K. Kim, Appl. Phys. Lett. **100**, 172413 (2012).

[69] R. Rückriem, T. Schrefl, and M. Albrecht, Appl. Phys. Lett. **104**, 052414 (2014).

[70] V. P. Kravchuk, Y. Gaididei, and D. D. Sheka, Phys. Rev. B **80**, 100405(R) (2009).

[71] S. Gliga, Y. Liu, and R. Hertel, J. Phys.:Conf. Ser. **303**, 012005 (2011).

[72] S. Zhang and Z. Li, Phys. Rev. Lett. **93**, 127204 (2004).

[73] H. Min, R. D. McMichael, M. J. Donahue, J. Miltat, and M. D. Stiles, Phys. Rev. Lett. **104**, 217201 (2010).

[74] B. Van de Wiele, L. Laurson, and G. Durin, Phys. Rev. B **86**, 144415 (2012).